A Novel Piezoelectric Strain Sensor for Simultaneous Damping and Tracking Control of a High-Speed Nanopositioner

Yuen Kuan Yong, *Member, IEEE*, Andrew J. Fleming, *Member, IEEE*, and S. O. Reza Moheimani, *Fellow, IEEE*

***Abstract*—This paper presents a novel piezoelectric strain sensor for damping and accurate tracking control of a high-speed nanopositioning stage. Piezoelectric sensors have the benefit of simple interface circuitry, low cost, high sensitivity, and high bandwidth. Although piezoelectric sensors have been successfully used as vibration sensors in smart structures, complications arise when they are used in a feedback loop for tracking. As piezoelectric strain sensors exhibit a capacitive source impedance, a high-pass filter is created, typically with a cut-off frequency of 1 to 10 Hz. This filter can cause significant errors and destabilize a tracking control system. Here, we overcome this problem by using a low-frequency bypass technique to replace the low-frequency component of the strain measurement with an estimate based on the open-loop system. Once the low-frequency filter is accounted for, any standard control system can be applied. In this paper, an analog integral resonant controller together with an integral tracking controller are implemented on a flexure-guided nanopositioner. The resulting closed-loop bandwidth is experimentally demonstrated to be 1.86 kHz. The nanopositioner is installed in an Atomic Force Microscope to obtain open- and closed-loop images at line rates of 40 and 78 Hz. Images recorded in closed loop show a significant improvement due to the elimination of nonlinearity.**

***Index Terms*—Atomic force microscope (AFM), control, high speed, nanopositioning, piezoelectric, strain sensor.**

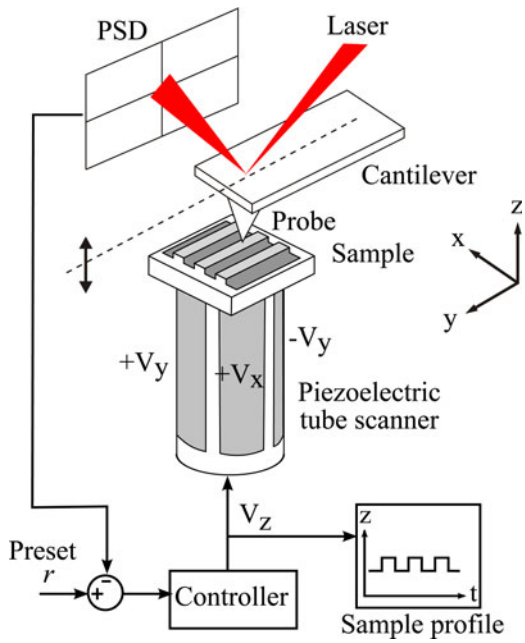

Fig. 1. Schematic of an AFM in constant force contact mode.

I. Introduction

THE atomic force microscope (AFM) has become an indispensable tool in many fields of nanotechnology, such as bioscience [1], [2], electrical characterization of semiconductors [3], micro/nanomanipulation [4]–[8] and nanoassembly [9]. In a typical scan-sample AFM, the sample is located on a piezoelectric tube scanner [10]. When operated in contact mode, a sharp probe on the free end of a microcantilever is brought into contact with the sample surface (see Fig. 1). The probe-sample interaction causes the cantilever to deflect. This deflection is measured using a laser source and a position sensitive diode (PSD). This deflection is compared with the set point value. A vertical feedback controller is used to minimize the difference between the measured and set point deflections by moving the Z-axis of the scanner. The scanner, on which a sample is placed, is moved in a raster pattern along its lateral axes. To generate the raster pattern, one axis of the scanner is required to track a triangular signal while the other axis is required to track a pseudostair signal. For constant-force contact mode scans (see Fig. 1), the vertical feedback controller remains activated to maintain the probe-sample interaction force during rastering. A topographic image of the sample surface is constructed from the electrical signal used to drive the Z-axis of the nanopositioner.

In recent years, there has been an increased demand for high-speed AFM in the areas of nanofabrication [11] and imaging of fast biological processes [12]. In order to achieve the required scanning speed and range, piezoelectric tube scanners have been replaced with flexure-based nanopositioners [13]–[17]. The two main drawbacks of flexure-based mechanisms are 1) the lightly damped resonant peaks, and 2) the nonlinearity of piezoelectric

Manuscript received April 21, 2011; revised August 23, 2011 and November 8, 2011; accepted March 27, 2012. Date of publication May 17, 2012; date of current version January 18, 2013. Recommended by Technical Editor G. Yang. This work was supported in part by a University of Newcastle Special Project Grant and in part by the Australia Research Council.

The authors are with the School of Electrical Engineering and Computer Science, The University of Newcastle, Callaghan, N.S.W. 2308, Australia (e-mail: yuenkuan.yong@newcastle.edu.au; andrew.fleming@newcastle.edu.au; reza.moheimani@newcastle.edu.au).

Color versions of one or more of the figures in this paper are available online at http://ieeexplore.ieee.org.

Digital Object Identifier 10.1109/TMECH.2012.2193895

stack actuators. The triangular waveform used to generate the raster pattern tends to excite the resonant peaks of a nanopositioner that in turn distort the AFM images. Further imaging artifacts arise from the positioning error caused by piezoelectric nonlinearity. Various feedforward and feedback control techniques have been successfully implemented to suppress vibration and compensate for nonlinearity [16], [18], [19], [20]. Feedback control systems typically employ capacitive or inductive position sensors that are usually limited in bandwidth to around 10 kHz. As the first resonance frequency of most high-speed nanopositioners is above 10 kHz [13], [14], [17], capacitive and inductive sensors are inadequate for control of high-speed nanopositioners. Furthermore, these sensors are typically expensive and physically large, making them difficult to install in a compact nanopositioner.

In this paper, a piezoelectric strain sensor is evaluated as an alternative position sensor for high-speed nanopositioning systems. Advantageously, piezoelectric sensors are extremely compact and can be bonded directly to flexures in order to measure displacement. Piezoelectric strain sensors also exhibit high sensitivity, wide bandwidth, and low noise at high frequencies [21], [22]. Due to their desirable characteristics, piezoelectric sensors are used widely for vibration sensing in smart structures [23]–[27]. Piezoelectric sensors have also been used to suppress the resonance of nanopositioning systems; however, additional sensors are still required for tracking control [28]–[30].

Although piezoelectric strain sensors have excellent ac properties, they cannot be used to measure low-frequency signals. This is due to the capacitive source impedance which introduces a high-pass filter with a typical cutoff frequency between 1 and 10 Hz. The high-pass filter can destabilize a standard tracking controller and severely affects the tracking accuracy at frequencies below ten times the cutoff frequency, that is, below approximately 10 to 100 Hz.

In this paper, the difficulties associated with the high-pass filter are avoided by implementing a low-frequency bypass technique. In this approach, the low-frequency component of the measured signal is replaced by an estimate based on the system input and an open-loop model [22]. The low-frequency bypass technique permits the direct application of standard controllers such as integral tracking or PID controllers.

It is known that the maximum bandwidth of an integral tracking controller is inversely proportional to the magnitude of the resonance peak [22], [31]. Hence, to achieve maximum bandwidth from the nanopositioner, the resonance is damped with an integral resonant controller (IRC) [32], [33] before the tracking controller is applied.

The remainder of the paper is organized as follows. A description of the experimental setup is provided in Section II. In Section III, the characteristics of the piezoelectric strain sensor are discussed. The relationship between the mechanical displacement and induced piezoelectric sensor voltage is derived analytically. The feedback control design is then discussed in Section IV followed by imaging experiments that demonstrate the effectiveness of the proposed techniques in Section V. Section VI concludes the paper.

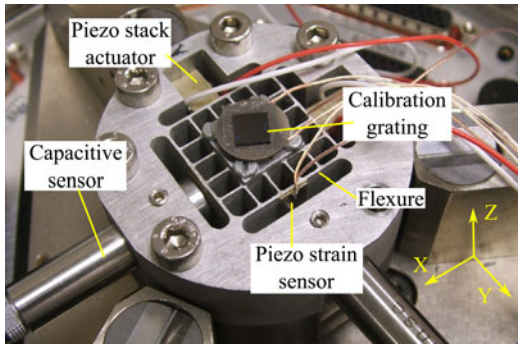

Fig. 2. *XYZ* nanopositioner with piezoelectric strain sensor. Two capacitive sensors are used to measure the displacement of the nanopositioner. The standoff distance between the capacitive sensor and its target is 0.1 mm. Note that the Y-axis capacitive sensor is retracted from its standoff position in order to clearly show the location of the piezoelectric strain sensor.

II. Experimental Setup

The piezoelectric tube scanner of a commercial AFM (NT-MDT NTEGRA) is replaced by a high-speed XYZ flexure-based nanopositioner as pictured in Fig. 2. The proposed sensing technique will be demonstrated on the fast-scanning axis of the nanopositioner. The X- and Y-axes of the nanopositioner are driven by Noliac SCMAP07 piezoelectric stack actuators (5 mm $\times$ 5 mm $\times$ 10 mm, 380 nF). The Z-axis is driven by a Noliac SCMAP06 stack actuator (3 mm $\times$ 3 mm $\times$ 6 mm, 70 nF). The nanopositioner has a motion range of 7 μm $\times$ 7 μm $\times$ 4 μm in the X-, Y-, and Z-axes, respectively. The first resonance frequency of the three axes is 11.3 kHz.

The piezoelectric strain sensor is a 5 mm $\times$ 10 mm $\times$ 0.25 mm plate of PI PIC151 piezoelectric ceramic bonded to the flexure with epoxy as shown in Fig. 2. The induced piezoelectric voltage was buffered by a unity-gain amplifier with an input impedance of 500 MΩ. Due to the 4.25-nF source capacitance of the sensor, the resulting high-pass cutoff frequency was 0.1 Hz. In order to calibrate the piezoelectric sensor, a MicroSense 6810 capacitive sensor with a sensitivity of 2.5 μm/V was also used to measure the displacement of the nanopositioner.

The Y-axis piezoelectric actuator was driven by a charge-drive with a gain of 10 μC/V and an equivalent voltage gain of 26. For the sake of comparison, the X-axis piezoelectric stack actuator was operated in open loop and driven using a voltage amplifier with a gain of 20. All frequency responses were recorded using a HP35670A dual-channel spectrum analyzer.

To evaluate the closed-loop imaging response, the nanopositioner was installed in an NT-MDT NTEGRA AFM. During imaging, the Y-axis of the nanopositioner was forced to track a fast triangular waveform and the X-axis was driven to follow a slow ramp signal.

III. Piezoelectric Strain Sensor

To measure the dynamic deflection of the nanopositioner, a piezoelectric plate is bonded to the flexure as shown in Fig. 3. Since the deflection is proportional to strain, the induced piezoelectric voltage is also proportional to deflection. This relationship is explored in the following.

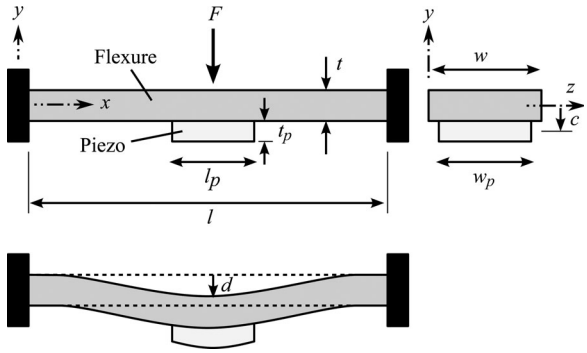

Fig. 3. Schematic diagram of a flexure with a bonded piezoelectric plate.

The voltage produced by the piezoelectric sensor is related to the strain in an Euler–Bernoulli beam. It is assumed that the beam is undergoing pure bending and the strain is constant along the z-axis in Fig. 3. If the piezoelectric actuator is modeled as a center-located point load, the transverse deflection $y(x)$ of a fixed–fixed uniform beam is known to be [34]

$$y(x) = \frac{F}{24EI}\left(2x^3 - \frac{3}{2}lx^2\right), \text{ for } 0 < x < \frac{l}{2} \tag{1}$$

where F is the applied force, E is the Young's modulus, and I is the moment of inertia. Although the aforementioned equation describes only one-half of the beam deflection, the deflection is symmetric about the midpoint. If the deflection d at the midpoint is known, (1) can be simplified to

$$y(x) = -d\frac{8}{l^3}\left(2x^3 - \frac{3}{2}lx^2\right), \text{ for } 0 < x < \frac{l}{2}. \tag{2}$$

Once the deflection is known, the induced piezoelectric voltage can be derived. For bending about the neutral axis of the beam, the strain is assumed to vary linearly along the y-axis in Fig. 3. The average strain at a section along the y-axis is assumed to be at the point c, where c is the distance from the neutral axis to the center of the piezoelectric sensor [24]. The strain S_1 in the sensor is

$$S_1(x) = -cy''(x) \tag{3}$$

where c is the distance to the neutral axis. The induced voltage v_p is [35]

$$v_p = K\frac{d_{31}E_p w_p}{C_p}\int_{l/2-l_p/2}^{l/2} S_1(x)\,dx \tag{4}$$

where K is a correction factor, E_p is the Young's Modulus of the piezoelectric material, w_p is the sensor width, d_{31} is the strain-charge coupling coefficient, and C_p is the capacitance given by $C_p = l_p w_p \varepsilon_{33}/t_p$, where t_p is the piezo thickness, l_p is the piezo length, and ε_{33} is the dielectric permittivity under constant stress. The correction factor $K = K_p K_b$ accounts for the lateral strain due to the Poisson coupling and the shear-lag effect of the bonding layer [35]. Sensors constructed from PZT are equally sensitive to lateral and longitudinal strain, so $K_p = (1-\nu)$ where ν is the Poisson ratio for aluminum (0.33) [35]. The shear-lag factor K_b is due to the bonding layer which reduces the strain experienced by the sensor. By assuming a bond layer with a thickness of 0.028 mm and a shear modulus of 300 MPa, the effective length and width fractions of the proposed sensor are 0.6783 and 0.8385, respectively. The equivalent area factor is $K_b = 0.6783 \times 0.8385 = 0.5688$. Thus, the correction factor K is approximately 0.3811.

TABLE I
PROPERTIES OF THE PIEZOELECTRIC STRAIN SENSOR AND THE FLEXURE DIMENSIONS

E_p GPa	d_{31} C/N	C_p nF	l_p mm	t_p mm	w_p mm
66	-210×10^{-12}	4.25	5	0.25	10

l mm	t mm	w mm	c mm
16	0.4	12.8	0.325

Since the deflection is symmetrical about the midpoint, the derivation of induced voltage can be simplified by considering a piezoelectric sensor that covers only one-half of the beam; that is, the length l_p is halved. Due to the symmetry about the midpoint, the induced voltage on the full sensor is equal to the half-sensor but with twice the capacitance. Taking this into account and combining (2) and (4) yields

$$\begin{aligned} v_p &= K\frac{d_{31}E_p w_p}{C_p/2}\left[-cy'(x)\right]_{\frac{l}{2}-\frac{l_p}{2}}^{\frac{l}{2}} \\ &= K\frac{d_{31}E_p w_p}{C_p/2}cd\frac{8}{l^3}\left[6x^2 - 3lx\right]_{\frac{l}{2}-\frac{l_p}{2}}^{\frac{l}{2}} \\ &= K\frac{d_{31}E_p w_p}{C_p/2}cd\frac{8}{l^3}\left(\frac{3ll_p}{2} - \frac{3l_p^2}{2}\right). \end{aligned} \tag{5}$$

Equation (5) demonstrates that the induced voltage is linearly proportional to the deflection of the nanopositioner. Parameters of the piezoelectric strain sensor and the flexure dimensions are listed in Table I.

To maximize the induced voltage produced by the sensor, the piezo should be located in the region of highest curvature. In this paper, maxima of curvature occur at the center. In addition to location, it is also desirable to maximize the capacitance of the sensor as this improves the low-frequency performance. To maximize capacitance, the lateral dimensions of the sensor should be as large as possible without covering any regions where the curvature changes phase. Hence, in this paper, the sensor is centrally located with the maximum practical dimensions listed in Table I.

From (5) and Table I, the estimated sensitivity is 1.3 V/μm of deflection at the midpoint. The experimentally measured sensitivity was 1.06 V/μm, which is lower than the predicted value. This discrepancy is due to the simplification of the analytical model where a center-located point load is used to derive the strain equation of the beam. In practice, forces transfer through a net structure and act on the beam via four vertical flexures. To model the strain of the beam accurately, four distributed loads should be used instead of a point load. However, this will make the analytical equation significantly more complex and contradict the original goal of deriving (5), which was to approximate the relationship between the strain and induced voltage.

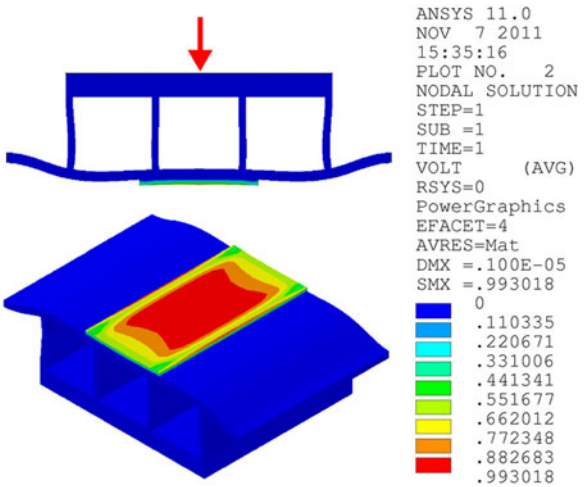

Fig. 4. FE-simulated piezoelectric strain-induced voltage. The simulated sensor sensitivity is 0.99 V/μm.

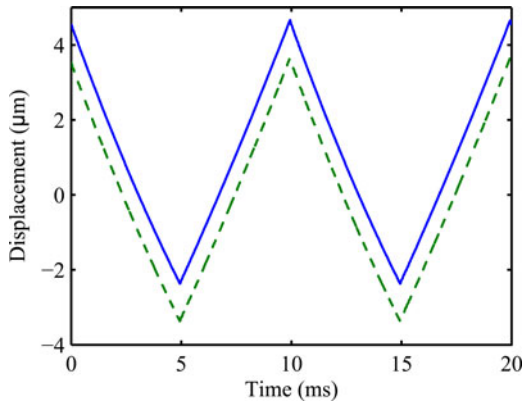

Fig. 5. Measured displacement in response to a full-range 100-Hz triangle wave (200 V). The solid line is the displacement measurement derived from the piezoelectric strain sensor V_s (–) while the dashed line is from the capacitive sensor d (- -). V_s is plotted with a 1-μm positive offset for the sake of clarity.

For a more accurate estimation, the sensor sensitivity can be predicted using a finite-element (FE) model. The FE model is constructed in ANSYS where the four vertical flexures are simulated (see Fig. 4). All flexures are modeled using SOLID45 elements. The element is defined by eight nodes and each node has three degree-of-freedoms (DOFs). Aluminium alloy Al7075 is used to fabricate the nanopositioner. Its Young's modulus and Poisson ratio are 72 GPa and 0.33, respectively. The piezoelectric sensor is modeled using SOLID5 elements. The element is a 3-D element that has eight nodes and six DOFs at each node. Properties of the piezoelectric material PI PIC151 are listed in Table I and can be found in [36]. A 0.028-mm thick bond layer between the flexure and the piezoelectric sensor is also modeled using SOLID45 elements with a shear modulus of 300 MPa. The same material property is used to estimate the correction factor K in (5). Fig. 4 shows the simulated piezoelectric sensor voltage when the flexure is experiencing 1-μm deflection at midlength. The simulated sensitivity is 0.99 V/μm, which is about 6% different from the experimental result. This could be due to the influence of the bonding layer where its thickness cannot be modeled accurately. Nevertheless, the FE result is in close agreement to that of the experiment.

A. Sensor Characteristics

Due to the capacitive nature of the piezoelectric sensor and the finite input impedance of electronics, the transfer function from v_p (the piezoelectric strain voltage) to V_s (measured voltage across the piezoelectric strain sensor) resembles a first-order high-pass filter H_p [22], that is

$$V_s = H_p(s)\, v_p, \quad \text{where } H_p(s) = \frac{s}{s+\omega_c} \tag{6}$$

where $\omega_c = 1/R_{\text{in}}C_p$, and R_{in} is the input impedance of the voltage buffer and C_p is the piezoelectric sensor capacitance. This high-pass characteristic causes a standard tracking controller to saturate.

To evaluate the sensor characteristics at dynamic frequencies, the frequency response functions (FRFs) of the nanopositioning system were recorded from the input applied to the charge amplifier to 1) the measured strain voltage $G_{vv}(i\omega)$ and 2) the measured displacement $G_{dv}(i\omega)$. Note that d is the displacement of the nanopositioner measured using a capacitive sensor. The two FRFs are plotted in Fig. 6. The first resonant peak of the system appears at 11.3 kHz in both plots.

To evaluate the linearity of the piezoelectric strain sensor, a 100-Hz triangular input signal of 200 V was applied to the actuator. Fig. 5 illustrates that the measured capacitive sensor signal is identical to the displacement derived from the piezoelectric strain sensor signal to within the limits of measurement.

IV. Modeling, Controller Design, and Implementation

To facilitate the controller design, a dynamic model is first required for the system. The nanopositioning system is considered to be a single-input two-output (SITO) system where the input is the applied voltage V_a and the outputs are displacement d and the piezoelectric strain voltage v_p. This SITO system is expressed as

$$\begin{bmatrix} d \\ v_p \end{bmatrix} = G(s)\, u, \quad \text{and} \quad G(s) = \begin{bmatrix} G_{dv}(s) \\ G_{vv}(s) \end{bmatrix}. \tag{7}$$

A second-order model was fitted to the measured frequency responses in Fig. 6 using the frequency-domain subspace algorithm [37]. The transfer functions of the two subsystems are

$$G_{vv}(s) = \frac{0.1662s^2 - 8569s + 2.684 \times 10^9}{s^2 + 5480s + 5.226 \times 10^9} \tag{8}$$

$$G_{dv}(s) = \frac{0.01825s^2 - 7453s + 1.105 \times 10^9}{s^2 + 5480s + 5.226 \times 10^9}. \tag{9}$$

The measured and modeled frequency responses of G_{vv} and G_{dv} are plotted in Fig. 6.

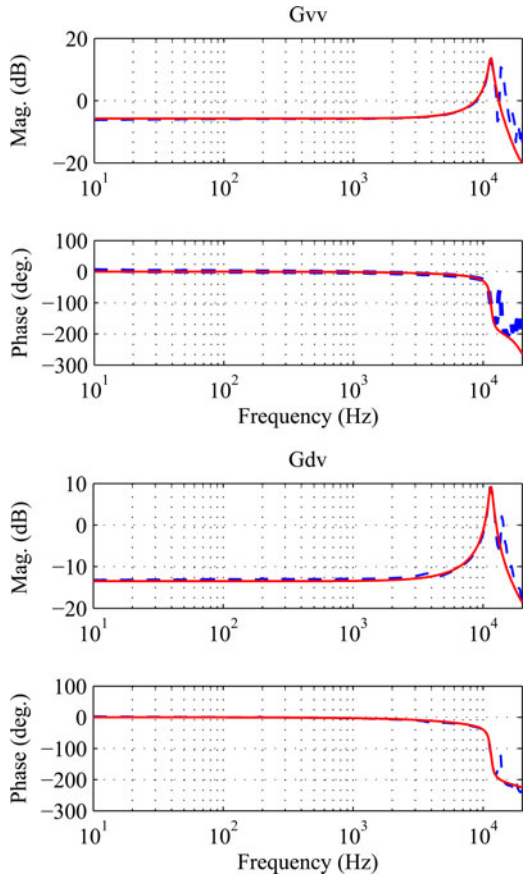

Fig. 6. Measured (- -) and modeled (–) frequency responses of G_{vv} and G_{dv}.

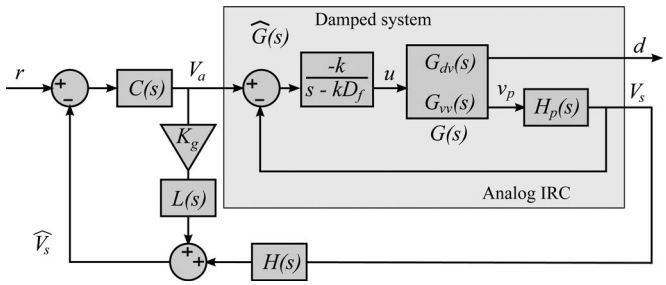

Fig. 7. Block diagram of the damped system $\widehat{G}(s)$ using the IRC and the low-frequency bypass control technique.

A. Damping Control

It is known that the bandwidth and stability margins of a standard tracking control system are inversely proportional to the magnitude of the lowest frequency resonance peak [33]. Hence, in order to maximize the closed-loop bandwidth of the nanopositioner, an IRC was designed to damp the first resonance mode. A block diagram of the system with IRC damping control is illustrated in Fig. 7. The shaded box in Fig. 7 represents the damped system $\widehat{G}(s)$. The IRC damping controller was designed by following the procedure in [32]. This procedure begins by finding a sufficiently large feedthrough term D_f so that the system zeros are lower than the resonance frequency. The new system with added feedthrough is referred to as $G_{vv}(s) + D_f$.

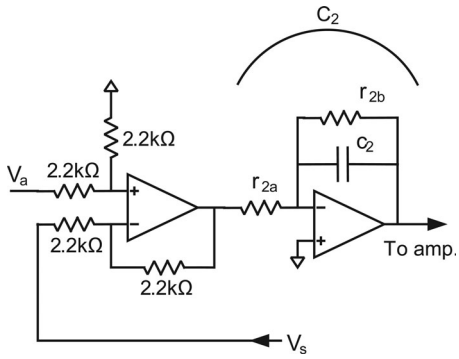

Fig. 8. Analog implementation of the IRC damping controller.

A suitable control gain k can then be found using the root-locus technique [33]. In this case, $D_f = -1$ and $k = 7 \times 10^4$ were used. Due to the high-mechanical resonance mode (11.3 kHz) and the limited sampling rate of the dSPACE prototyping system, the IRC controller was implemented in analog form [33]. Although the transfer function can be implemented by a single op-amp, the dual configuration, shown in Fig. 8, is simpler to tune if necessary.

The first stage of the circuit in Fig. 8 is a unity-gain differential amplifier. The IRC is implemented by the inverting integrator stage C_2, where

$$C_2 = \frac{-k}{s - kD_f}. \tag{10}$$

The circuit transfer function is

$$\frac{-\frac{1}{r_{2a}c_2}}{s + \frac{1}{r_{2b}c_2}}. \tag{11}$$

As k is positive and D_f is negative, the equalities are

$$r_{2a}c_2 = \frac{1}{k}, \text{ and } r_{2b}c_2 = \frac{1}{-kD_f}. \tag{12}$$

The component values $r_{2a} = r_{2b} = 4.33$ kΩ and $c_2 = 3.3$ nF are used to implement the controller. The op-amp is an LT1362. However, almost any general purpose high-speed op-amp would be suitable.

B. Tracking Control

As discussed in Section III-A, the high-pass characteristic of the piezoelectric strain voltage precludes the direct use of an integral tracking controller. In this paper, we use the low-frequency bypass technique [22] that allows the piezoelectric strain voltage to be used for tracking. In this technique, the complementary low-pass filter $L(s)$ and high-pass filter $H(s)$ (see Fig. 7) are used to substitute the actual output with an estimate at frequencies below the crossover frequency α, chosen to be 10 Hz. Since the filters are complementary, they sum to unity and do not add dynamics to the control loop. The filters are chosen to be first order so that they are easily constructed as an analog circuit. The transfer functions of the complementary

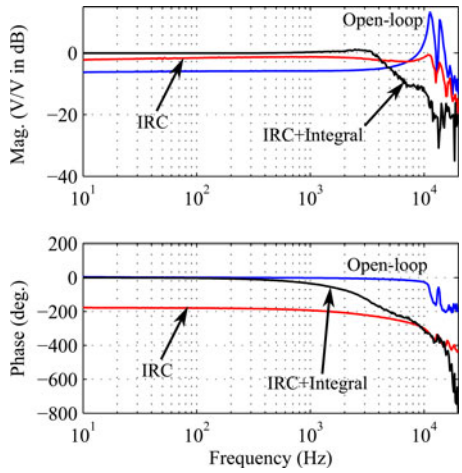

Fig. 9. Measured frequency responses of the open-loop system, the damped system with IRC, and the closed-loop system with IRC and integral tracking control.

filters are

$$H(s) = \frac{s}{(s+\alpha)}, \text{ and } L(s) = 1 - H_p(s) H(s) \qquad (13)$$

where $H_p(s)$ is the high-pass filter associated with the piezoelectric strain voltage defined in (6) that has a cutoff frequency of 0.1 Hz. The signal V_a is scaled to have the same sensitivity as V_s by a constant K_g. Providing K_g is accurately tuned, the transfer function from r to V_s is

$$\frac{V_s}{r} = \frac{C(s)\widehat{G}_{vv}(s)}{1 + C(s)\left(K_g L(s) + \widehat{G}_{vv}(s) H(s)\right)} \qquad (14)$$

where $C(s)$ is a negative integral controller, $C(s) = -k_i/s$. The transfer function from r to d is

$$\frac{d}{r} = \frac{C(s)\widehat{G}_{dv}(s)}{1 + C(s)\left(K_g L(s) + \widehat{G}_{vv}(s) H(s)\right)}. \qquad (15)$$

Piezoelectric stack actuators exhibit significant hysteresis when driven with large voltages. This can cause the system sensitivity and K_g to be dependent on the voltage magnitude. However, in this paper, a charge drive [38] is used to minimize hysteresis. K_g was successfully tuned to -1.05. An alternative method to account for the presence of hysteresis involves the inclusion of a nonlinear model in K_g. The Preisach model [39], Prandtl–Ishlinskii operator [40], and Maxwell resistive capacitor model [41] have all been used to effectively model low-frequency hysteresis.

The experimental frequency responses of the open-loop, damped, and closed-loop system are plotted in Fig. 9. The resulting tracking bandwidth of the closed-loop system is 1.86 kHz (45° phase lag) when using an integral gain of k_i =15 000. The gain and phase margins are 11.3 dB and 58.6°, respectively. Without the IRC damping controller, the maximum tracking bandwidth is reduced to 956 Hz (k_i =12 000) with a gain margin of only 2.7 dB. Thus, by using a damping controller, the tracking bandwidth and gain margin are successfully increased by a factor of 2 and 2.7, respectively.

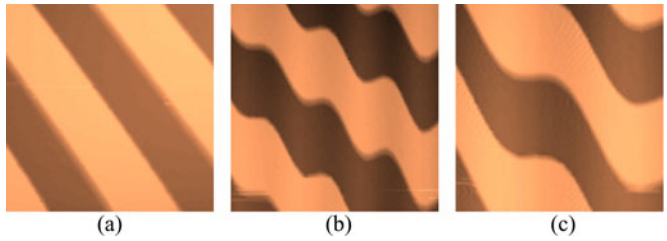

Fig. 10. AFM images recorded using a commercial piezoelectric tube scanner at line rates (a) 1 Hz, (b) 40 Hz, and (c) 78 Hz.

The closed-loop time-domain performance was evaluated by driving the nanopositioner with a full-range (200 V) triangle wave. The open- and closed-loop responses are plotted in Fig. 11. When tracking the triangular reference, the nonlinearity is effectively suppressed with negligible tracking lag. Good tracking performance was observed up to around 10% of the bandwidth, or approximately 180 Hz. In addition to hysteresis rejection, some applications also require immunity from creep. In high-speed AFM, the scanning signals do not contain dc or low-frequency components, so creep is not an issue. However, if the scan speed was reduced below 1 Hz, creep could begin to degrade the accuracy. If immunity to creep is required, the static gain K_g could be augmented with an appropriate model. Previous research has shown that creep can be adequately modeled by a third-order linear system [39].

V. AFM Imaging Performance

To demonstrate the efficacy of the proposed control strategy, this section presents AFM images of a MikroMasch TGZ2 calibration grating with a period of 3 μm and a step height of 108 nm. This grating is useful for quantifying the imaging artifacts that arise from the scanner nonlinearity. All images were recorded in constant-force contact-mode. The cantilever was a BudgetSensors ContAl probe with a resonance frequency of 13 kHz and stiffness of 0.2 N/m.

Open-loop images obtained using a commercial AFM piezoelectric tube scanner are plotted in Fig. 10. With its in-built nonlinearity compensation technique activated, a good quality image was obtained at 1-Hz line rate. The piezoelectric tube scanner has the first lateral resonance frequency at 580 Hz. To avoid triggering the resonant modes of the tube scanner, images are often scanned at 1% of the tube scanner's lowest resonance frequency. This amounts to a maximum line rate of 5.8 Hz. To demonstrate the limitation of the piezoelectric tube scanner at high speed, images were recorded at 40- and 78-Hz line rates. Vibration-induced artifacts are observed where the images are severely distorted at these frequencies (see Fig. 10).

In this paper, the piezoelectric tube scanner is replaced by the flexure-based nanopositioner which has its first lateral resonance frequency at 11.3 kHz. Fig. 11 shows the open- and closed-loop images obtained using the flexure-based nanopositioner at line rates of 40 and 78 Hz. Vibration-induced artifacts are not noticeable in all images. The skewed edges of the images are due to the cross coupling between the X- and Y-axes that slightly reduces the full-range scan area. The effect of cross

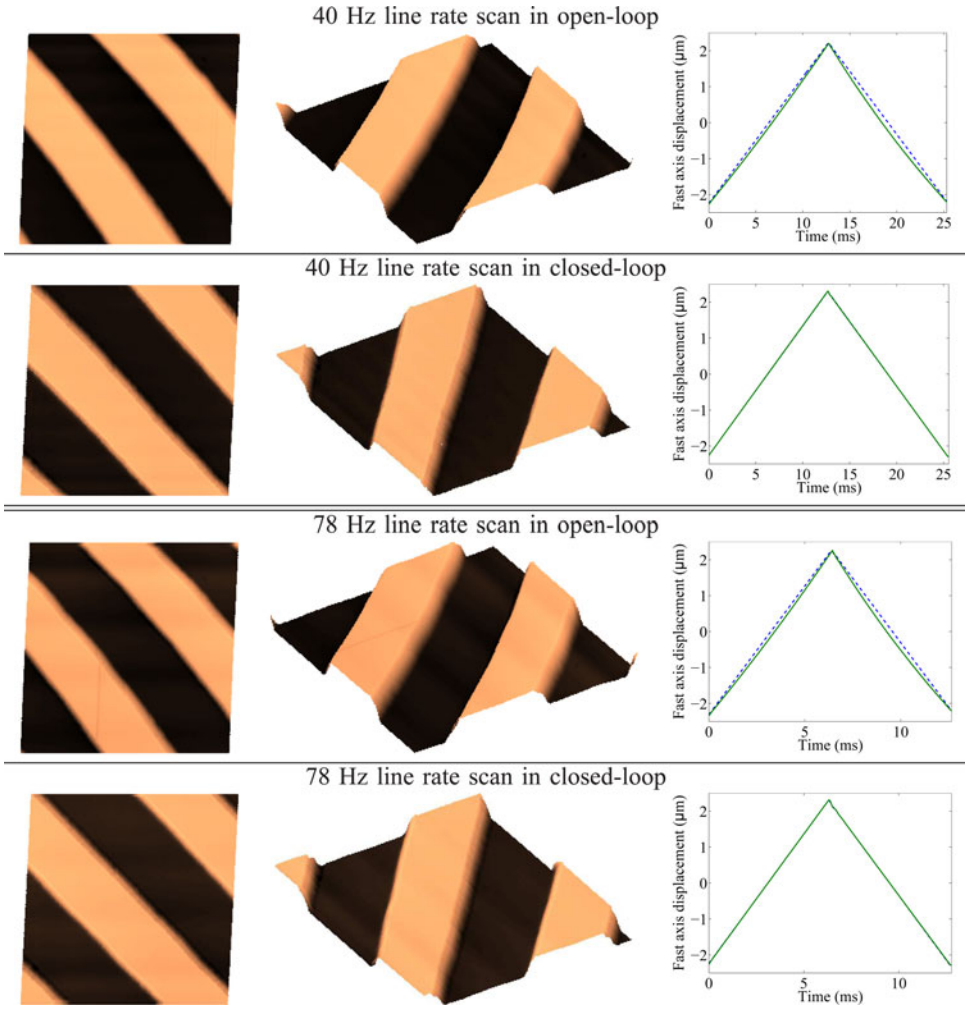

Fig. 11. Open- and closed-loop AFM images recorded at 40- and 78-Hz line rate. For the displacement plots, the reference signal is plotted in dotted line and the displacement measurement derived from the piezoelectric strain sensor is plotted in solid line.

TABLE II
OPEN- AND CLOSED-LOOP TRACKING ERRORS (IN NANOMETER) AT 40- AND 78-HZ LINE RATES

Line rate	Open-loop		Closed-loop	
(Hz)	Max.	RMS	Max.	RMS
40	224.4	136.7	38.5	15.3
78	239.0	139.5	41.2	14.0

coupling on AFM images can be minimized by implementing feedback-control methods [16], [42] or by postprocessing image data offline [43]. In open loop, the hysteresis effect of the piezoelectric stack actuator is minimized by the charge drive but not completely eliminated. The remnant nonlinearity is noticeable in the open-loop scans where the features appear curved. The nonlinearity is also visible in the measured displacement plot.

Scans recorded in closed loop show significant improvement due to the reduction of nonlinearity. With the high tracking bandwidth achieved by the proposed control strategy, the closed-loop system does not exhibit tracking lag while following a 78-Hz triangular reference. As shown in Table II, the maximum and RMS tracking errors in closed loop are significantly smaller than that in open loop for both scan rates.

VI. CONCLUSION

In this paper, a piezoelectric strain sensor was bonded to a flexure-based nanopositioner as a displacement sensor for damping and tracking control. Compared to existing sensors, such as capacitive sensors, piezoelectric strain sensors are extremely low cost, simple, compact, have a very high bandwidth, and produce low noise at high frequencies. However, they also exhibit a high-pass characteristic at low frequencies that precludes their use in a tracking control system.

In this paper, problems associated with the high-pass characteristic of a piezoelectric sensor are eliminated by using a pair of complementary filters to replace the piezoelectric signal at low frequencies with a displacement estimate based on the present input and an open-loop model.

An analog IRC damping controller was designed and implemented to suppress the first resonance mode of the nanopositioner. With damping and integral tracking control, a closed-loop bandwidth of 1.86 kHz was achieved.

The improvements to AFM imaging performance were demonstrated by installing the proposed nanopositioner in a commercial scanning probe microscope. The closed-loop

images are free from artifacts caused by scanner nonlinearity, even at scan rates of 78 Hz. These experimental results demonstrate the efficacy of using a piezoelectric strain sensor for damping and tracking control of high-speed nanopositioners.

ACKNOWLEDGMENT

The research was performed at the Laboratory for Dynamics and Control of Nanosystems at the University of Newcastle.

REFERENCES

[1] T. Ando, T. Uchihashi, and T. Fukuma, "High-speed atomic force microscopy for nano-visualization of dynamic biomolecular processes," *Progr. Surf. Sci.*, vol. 83, no. 7–9, pp. 337–437, 2008.

[2] H. Yamashita, N. Kodera, A. Miyagi, T. Uchihashi, D. Yamamoto, and T. Ando, "Tip-sample distance control using photothermal actuation of a small cantilever for high-speed atomic force microscopy," *Rev. Sci. Instrum.*, vol. 78, no. 8, pp. 083702-1–083702-6, 2007.

[3] R. A. Oliver, "Advances in afm for the electrical characterization of semiconductors," *Rep. Progr. Phys.*, vol. 71, no. 7, p. 076501, 2008.

[4] J. M. Rodriguez-Fortun, J. Orus, J. Alfonso, F. B. Gimeno, and J. A. Castellanos, "Flatness-based active vibration control for piezoelectric actuators," *IEEE/ASME Trans. Mechatronics*, [Online]. Available: ieeexplore.ieee.org, DOI: 10.1109/TMECH.2011.2166998.

[5] H. C. Liaw and B. Shirinzadeh, "Neural network motion tracking control of piezo-actuated flexure-based mechanisms for micro-/nanomanipulation," *IEEE/ASME Trans. Mechatronics*, vol. 14, no. 5, pp. 517–527, Oct. 2009.

[6] G. Jayanth and C.-H. Menq, "Modeling and design of a magnetically actuated two-axis compliant micromanipulator for nanomanipulation," *IEEE/ASME Trans. Mechatronics*, vol. 15, no. 3, pp. 360–370, Jun. 2010.

[7] G. Jayanth and C.-H. Menq, "Control of a two-axis micromanipulator-based scanning probe system for 2.5-d nanometrology," *IEEE/ASME Trans. Mechatronics*, vol. 15, no. 5, pp. 661–670, Oct. 2010.

[8] Y. K. Yong, T.-F. Lu, and D. C. Handley, "Review of circular flexure hinge design equations and derivation of empirical formulations," *Precision Eng.*, vol. 32, no. 2, pp. 63–70, 2008.

[9] F. Krohs, C. Onal, M. Sitti, and S. Fatikow, "Towards automated nanoassembly with the atomic force microscope: A versatile drift compensation procedure," *J. Dyn. Syst., Meas., Control*, vol. 131, no. 6, p. 061106, 2009.

[10] G. Binnig and D. P. E. Smith, "Single-tube three-dimensional scanner for scanning tunneling microscopy," *Rev. Sci. Instrum.*, vol. 57, no. 8, pp. 1688–1689, 1986.

[11] J. A. Vicary and M. J. Miles, "Real-time nanofabrication with high-speed atomic force microscopy," *Nanotechnol.*, vol. 20, no. 9, p. 095302, 2009.

[12] N. Kodera, H. Yamashita, and T. Ando, "Active damping of the scanner for high-speed atomic force microscopy," *Rev. Sci. Instrum.*, vol. 76, no. 5, pp. 053708-1–053708-5, 2005.

[13] T. Ando, T. Uchihashi, N. Kodera, D. Yamamoto, A. Miyagi, M. Taniguchi, and H. Yamashita, "High-speed AFM and nano-visualization of biomolecular processes," *Pflügers Archiv. Eur. J. Physiol.*, vol. 456, no. 1, pp. 211–225, 2008.

[14] G. Schitter, K. J. Åstrom, B. DeMartini, P. J. Thurner, K. L. Turner, and P. K. Hansma, "Design and modeling of a high-speed AFM-scanner," *IEEE Trans. Control Syst. Technol.*, vol. 15, no. 5, pp. 906–915, Sep. 2007.

[15] Y. K. Yong, S. Aphale, and S. O. R. Moheimani, "Design, identification and control of a flexure-based XY stage for fast nanoscale positioning," *IEEE Trans. Nanotechnol.*, vol. 8, no. 1, pp. 46–54, Jan. 2009.

[16] Y. K. Yong, K. Liu, and S. O. R. Moheimani, "Reducing cross-coupling in a compliant XY nanopositioning stage for fast and accurate raster scanning," *IEEE Trans. Control Syst. Technol.*, vol. 18, no. 5, pp. 1172–1179, Sep. 2010.

[17] B. J. Kenton and K. K. Leang, "Design and control of a three-axis serial-kinematic high-bandwidth nanopositioner," *IEEE/ASME Trans. Mechatronics*, vol. 17, no. 2, pp. 356–369, Apr. 2012.

[18] G. M. Clayton, S. Tien, K. K. Leang, Q. Zou, and S. Devasia, "A review of feedforward control approaches in nanopositioning for high-speed SPM," *J. Dyn. Syst., Meas., Control*, vol. 131, no. 6, pp. 061101-1–061101-19, 2009.

[19] K. K. Leang and S. Devasia, "Feedback-linearized inverse feedforward for creep, hysteresis, and vibration compensation in piezoactuators," *IEEE Control Syst. Technol.* (Special Issue on Dynamic Control of Micro- and Nano-Scale Systems), vol. 15, no. 5, pp. 927–935, Sep. 2007.

[20] S. Devasia, E. Eleftheriou, and S. O. R. Moheimani, "A survey of control issues in nanopositioning," *IEEE Trans. Control Syst. Technol.*, vol. 15, no. 5, pp. 802–823, Sep. 2007.

[21] A. J. Fleming, A. Wills, and S. O. R. Moheimani, "Sensor fusion for improved control of piezoelectric tube scanners," *IEEE Trans. Control Syst. Technol.*, vol. 16, no. 6, pp. 1265–1276, Nov. 2008.

[22] A. J. Fleming, "Nanopositioning system with force feedback for high-performance tracking and vibration control," *IEEE/ASME Trans. Mechatronics*, vol. 15, no. 3, pp. 433–447, Jun. 2010.

[23] J. L. Fanson and T. K. Caughey, "Positive position feedback control for large space structures," *AIAA J.*, vol. 28, no. 4, pp. 717–724, 1990.

[24] J. J. Dosch, D. J. Inman, and E. Garcia, "A self-sensing piezoelectric actuator for collocated control," *J. Intell. Mater. Syst. Struct.*, vol. 3, no. 1, pp. 166–185, 1992.

[25] A. J. Fleming and S. O. R. Moheimani, "Control oriented synthesis of high performance piezoelectric shunt impedances for structural vibration control," *IEEE Trans. Control Syst. Technol.*, vol. 13, no. 1, pp. 98–112, Jan. 2005.

[26] S. Kuiper and G. Schitter, "Active damping of a piezoelectric tube scanner using self-sensing piezo actuation," *Mechatronics*, vol. 20, no. 6, pp. 656–665, 2010.

[27] S. O. R. Moheimani, "Invited review article: Accurate and fast nanopositioning with piezoelectric tube scanners: Emerging trends and future challenges," *Rev. Sci. Instrum.*, vol. 79, no. 7, pp. 071101-1–071101-11, 2008.

[28] A. J. Fleming and K. K. Leang, "Integrated strain and force feedback for high performance control of piezoelectric actuators," *Sens. Actuat. A*, vol. 161, no. 1–2, pp. 256–265, 2010.

[29] G. Schitter, P. J. Thurner, and P. K. Hansma, "Design and input-shaping control of a novel scanner for high-speed atomic force microscopy," *Mechatronics*, vol. 18, pp. 282–288, 2008.

[30] I. A. Mahmood, S. O. R. Moheimani, and K. Liu, "Tracking control of a nanopositioner using complementary sensors," *IEEE Trans. Nanotechnol.*, vol. 8, no. 1, pp. 55–65, Jan. 2009.

[31] A. Fleming, "Dual-stage vertical feedback for high-speed scanning probe microscopy," *IEEE Trans. Control Syst. Technol.*, vol. 19, no. 1, pp. 156–165, Jan. 2011.

[32] S. S. Aphale, A. J. Fleming, and S. O. R. Moheimani, "Integral resonant control of collocated smart structures," *Smart Mater. Struct.*, vol. 16, pp. 439–446, 2007.

[33] A. J. Fleming, S. Aphale, and S. O. R. Moheimani, "A new method for robust damping and tracking control of scanning probe microscope positioning stages," *IEEE Trans. Nanotechnol.*, vol. 9, no. 4, pp. 438–448, Jul. 2010.

[34] J. E. Shigley and C. R. Mischke, *Mechanical Engineering Design*. New York: McGraw-Hill, 1989.

[35] J. Sirohi and I. Chopra, "Fundamental understanding of piezoelectric strain sensors," *J. Intell. Mater. Syst. Struct.*, vol. 11, no. 4, pp. 246–257, 2000.

[36] *MicroPositioning, NanoPositioning, NanoAutomation. Solutions for Cutting-Edge Technologies.* Physik Instrumente Catalog, Karlsruhe, Germany, 2010.

[37] T. McKelvey, H. Akcay, and L. Ljung, "Subspace based multivariable system identification from frequency response data," *IEEE Trans. Automat. Control*, vol. 41, no. 7, pp. 960–978, Jul. 1996.

[38] A. J. Fleming and K. K. Leang, "Charge drives for scanning probe microscope positioning stages," *Ultramicroscopy*, vol. 108, no. 12, pp. 1551–1557, 2008.

[39] D. Croft, G. Shedd, and S. Devasia, "Creep, hysteresis, and vibration compensation for. piezoactuators: Atomic force microscopy application," *J. Dyn. Syst., Meas., Control*, vol. 123, no. 1, pp. 35–43, 2001.

[40] M. Al Janaideh, S. Rakheja, and C.-Y. Su, "An analytical generalized prandtl-ishlinskii model inversion for hysteresis compensation in micropositioning control," *IEEE/ASME Trans. Mechatronics*, vol. 16, no. 4, pp. 734–744, Aug. 2011.

[41] T.-J. Yeh, S.-W. Lu, and T.-Y. Wu, "Modeling and identification of hysteresis in piezoelectric actuators," *J. Dyn. Syst., Meas., Control*, vol. 128, no. 2, pp. 189–196, 2006.

[42] I. A. Mahmood and S. O. R. Moheimani, "Making a commercial AFM more accurate and faster using positive position feedback control," *Rev. Sci. Instrum.*, vol. 80, no. 6, pp. 063705-1–063705-8, 2009.

[43] Y. Sun and J. H. L. Pang, "AFM image reconstruction for deformation measurements by digital image correlation," *Nanotechnology*, vol. 17, pp. 933–939, 2006.

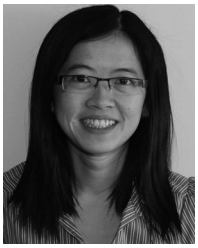

Yuen Kuan Yong (M'09) received the B.Eng. degree (1st Class Hons.) in mechatronic engineering and the Ph.D. degree in mechanical engineering from The University of Adelaide, Adelaide, Australia, in 2001 and 2007, respectively.

She is currently a Postdoctoral Research Fellow at The University of Newcastle, Callaghan, Australia. Her research interests include the design and control of nanopositioning systems, high-speed atomic force microscopy, finite-element analysis of smart materials and structures, and sensing and actuation.

Dr. Yong was a recipient of the 2008 IEEE/ASME International Conference on Advanced Intelligent Mechatronics (AIM) Best Conference Paper Finalist Award. She is a member of the Technical Program Committee of AIM and the International Conference on Manipulation, Manufacturing, and Measurement on the Nanoscale (3M-NANO). She is also a member of the Editorial Board of the *International Journal of Advanced Robotic Systems*.

Andrew J. Fleming (M'02) was born in Dingwall, U.K., in 1977. He received the Bachelor's degree in electrical engineering in 2000 and the Ph.D. degree in 2004 from The University of Newcastle, Callaghan, Australia.

He is currently an Australian Research Council Fellow in the School of Electrical Engineering and Computer Science, The University of Newcastle. He is the coauthor of two books, several patent applications, and more than 100 journal and conference papers. His research interests include nanopositioning, high-speed scanning probe microscopy, and microcantilever sensors.

Dr. Fleming was awarded The University of Newcastle Vice-Chancellors Award for Researcher of the Year and the Faculty of Engineering and Built Environment Award for Research Excellence in 2007. Also in 2007, he was a recipient of the IEEE Control Systems Society Outstanding Paper Award for research published in the IEEE TRANSACTIONS ON CONTROL SYSTEMS TECHNOLOGY.

S. O. Reza Moheimani (F'11) received the Ph.D. degree in electrical engineering from the University of New South Wales at the Australian Defence Force Academy, Canberra, Australia, in 1996.

He joined The University of Newcastle, Callaghan, Australia, in 1997, where he founded and directs the Laboratory for Dynamics and Control of Nanosystems, a multi-million-dollar state-of-the-art research facility. He is also a Professor and an Australian Research Council Future Fellow with the School of Electrical Engineering and Computer Science,The University of Newcastle. His current research interests include the area of dynamics and control at the nanometer scale, and applications of control and estimation in nanopositioning systems for high-speed scanning probe microscopy, modeling and control of microcantilever-based devices, control of microactuators in microelectromechanical systems, and control issues related to ultrahigh-density probe-based data storage systems.

Prof. Moheimani is a corecipient of the 2007 IEEE TRANSACTIONS ON CONTROL SYSTEMS TECHNOLOGY Outstanding Paper Award, and the 2009 IEEE CSS Control Systems Technology Award; the latter with a group of researchers from IBM Zurich Research Labs, where he has held several visiting appointments. He has served on the Editorial Board of a number of journals including the IEEE TRANSACTIONS ON CONTROL SYSTEMS TECHNOLOGY, the IEEE/ASME TRANSACTIONS ON MECHATRONICS, and *Control Engineering Practice*, and has chaired several international conferences and workshops. He currently chairs the IFAC Technical Committee on Mechatronic Systems. He is a Fellow of the International Federation of Automatic Control and of the Institute of Physics (U.K.).